Electronic Supplementary Information

Excellent OER electrocatalyst of cubic $SrCoO_{3-\delta}$ prepared by a simple F-doping strategy

*Wanhua Wang,[a] Yi Yang,[a] Daoming Huan,[a] Likun Wang,[b] Nai Shi,[a] Yun Xie,[a] Changrong Xia,[a] Ranran Peng,[*a,c,d] Yalin Lu[*a,c,d,e]*

[a.] *CAS Key Laboratory of Materials for Energy Conversion, Department of Materials Science and Engineering, University of Science and Technology of China, Hefei, 230026 Anhui, China. pengrr@ustc.edu.cn; yllu@ustc.edu.cn*

[b.] *Department of Materials Science and Chemical Engineering, State University of New York at Stony Brook, Stony Brook, New York 11794, United States.*

[c.] *Synergetic Innovation Center of Quantum Information & Quantum Physics, University of Science and Technology of China, Hefei, Anhui 230026, China.*

[d.] *Hefei National Laboratory of Physical Science at the Microscale, University of Science and Technology of China, Hefei, 230026 Anhui, China.*

[e.] *National Synchrotron Radiation Laboratory, University of Science and Technology of China, Hefei 230026, P. R. China.*

[*]*: Corresponding author*

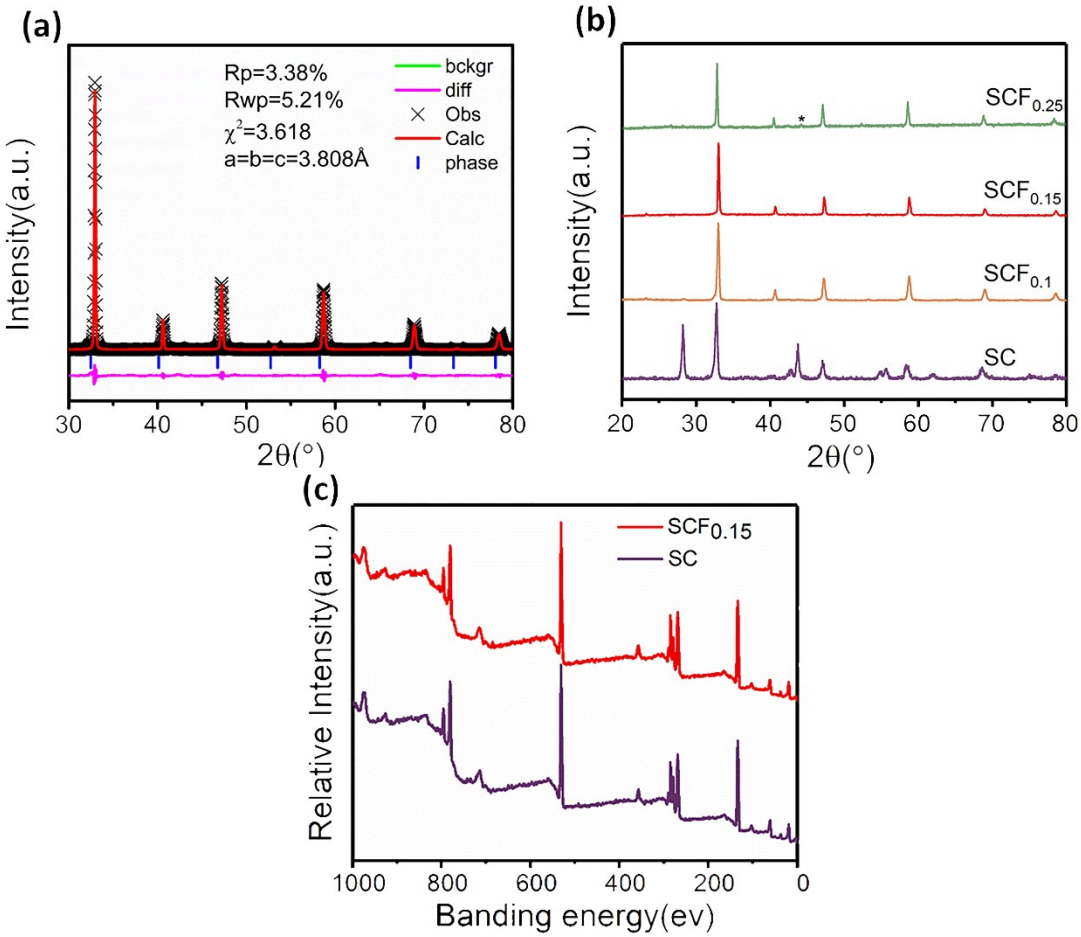

Figure S1. (a) RT-XRD patterns of $SCF_{0.15}$. (b) XRD of the as prepared $SCF_{0.25}$, $SCF_{0.15}$, $SCF_{0.1}$ and SC samples. (c) XPS wide-scan spectrum of as prepared $SCF_{0.15}$ and SC powder.

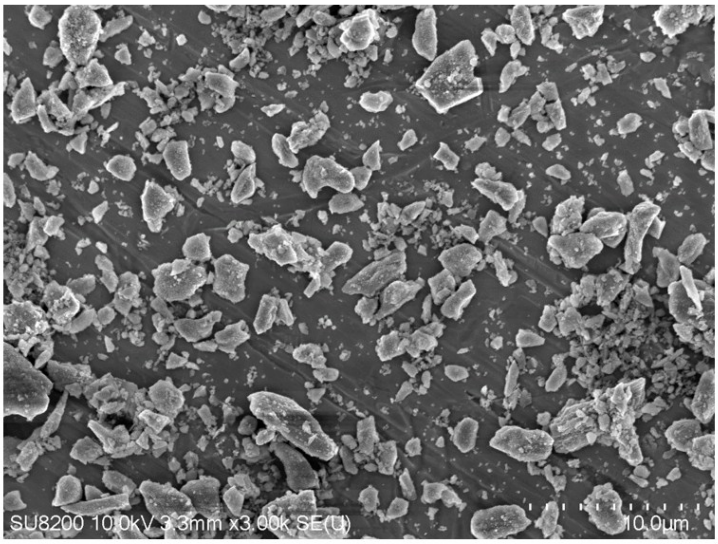

Figure S2. SEM picture of $SCF_{0.15}$ powder

The average grain size of $SCF_{0.15}$ powders is about 3μm from the SEM picture.

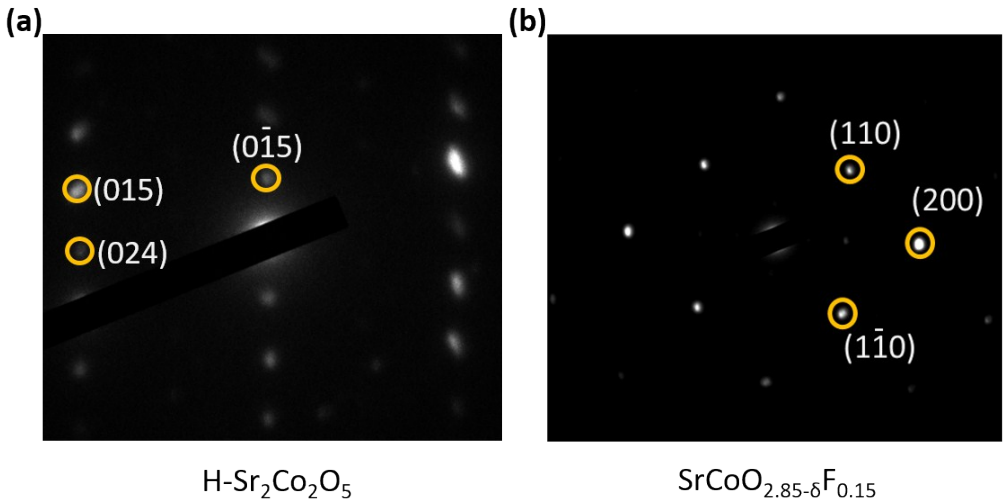

Figure S3. (a) Selected-area electron diffraction (SAED) patterns along the [100] zone axis of (a) H-$Sr_2Co_2O_5$ and (b) $SrCoO_{2.85-\delta}F_{0.15}$.

Figure S3 shows the SAED patterns for H-$Sr_2Co_2O_5$ and $SrCoO_{2.85-\delta}F_{0.15}$, further demonstrate the phase transformation from hexagonal to cubic perovskite phase after F-doping.

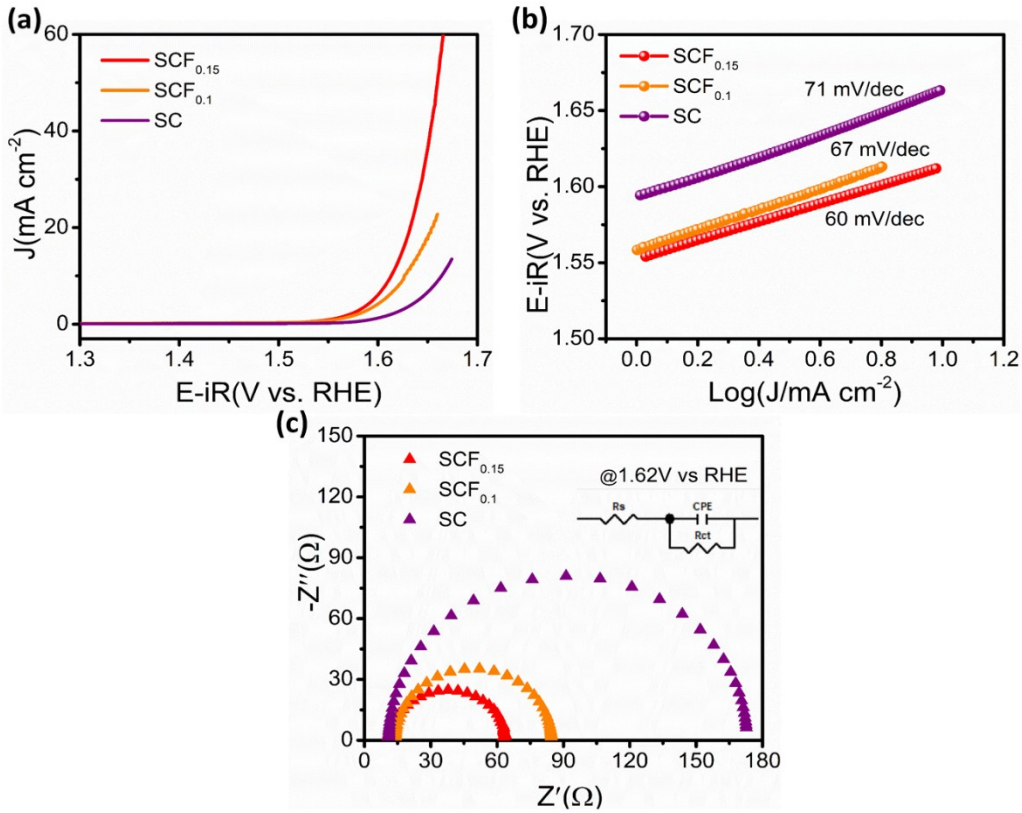

Figure S4. (a) The IR-corrected linear sweep voltammogram (LSV) OER curves of $SCF_{0.15}$, $SCF_{0.1}$, and SC catalysts in O_2-saturated 1 M KOH solutions. (b) The IR-corrected Tafel plots of various catalysts. (c) EIS Nyquist plots of $SCF_{0.15}$, $SCF_{0.1}$ and SC electrocatalysts recorded at OER potential of 1.62 V (vs RHE).

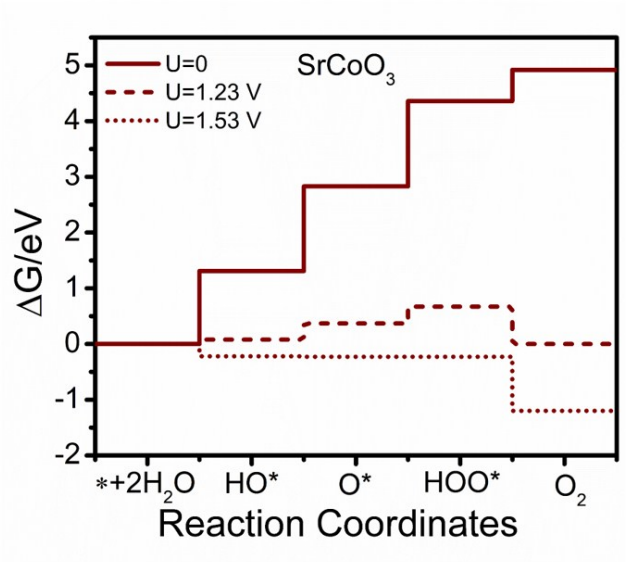

Figure S5. Standard free energy diagrams for OER obtained at zero potential (U=0), equilibrium potential for OER (U=1.23 V), and at the potential for which all steps proceed downward at pH 14 and T=298 K.

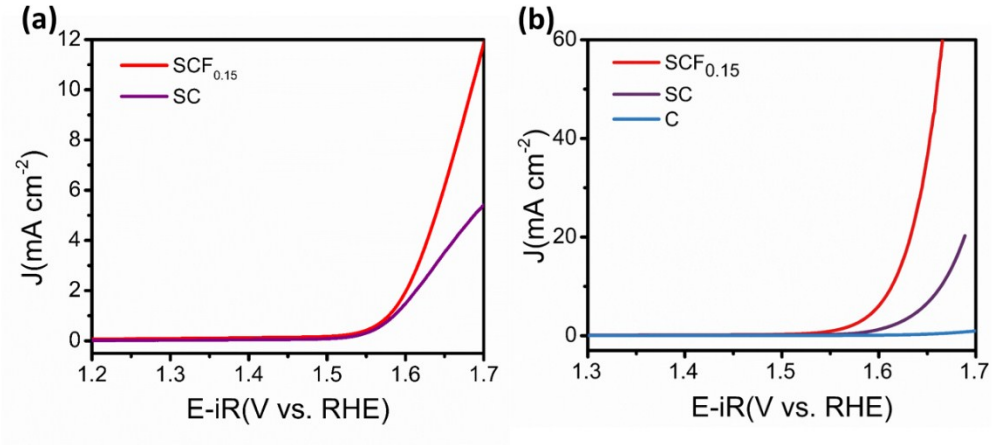

Figure S6. The IR-corrected linear sweep voltammogram (LSV) OER curves of $SCF_{0.15}$ and SC catalysts (a) without and (b) with carbon black in O_2-saturated 1 M KOH solutions.

In order to state the impact of electrical conductivity on catalytic performance, we prepared the pure $SCF_{0.15}$ and SC catalyst electrodes (without carbon black), and then tested their OER activities. As shown in the figure S6(a), compared with those using carbon black (figure S6(b)), large performance reductions can be clearly observed for both electrodes without carbon black. This result indicates that the high electrical conductivity of carbon black, in spite of its negligible electrocatalytic activity, contributes much to the performance improvement of $SCF_{0.15}$ and SC catalysts. Based on this result, it can be deduced that the higher electrical conductivity of $SCF_{0.15}$ over SC should also contributes to the better native performance of $SCF_{0.15}$ electrode, in addition to its better electrocatalytic activity toward OER.

Table 1. O 1s XPS peak deconvolution results

Electrocatalysts	Lattice O^{2-}	O_2^{2-}/O^-	-OH or O_2	H_2O or CO_3^{2-}
$SCF_{0.15}$	10.4%	39.33%	43.26%	7.01%
$SCF_{0.1}$	11%	27.5%	53.6%	7.9%
SC	24.49%	11.19%	56.48%	7.84%

Table 2. Comparisons of the IR-corrected OER activities of $SCF_{0.15}$ catalyst with other famous perovskite electrocatalysts in 1 M KOH saturated with O_2

Catalyst	Tafel slope (mV/dec)	Overpotential at 10 mA/cm^2 (mV)	Reference
$SrCoO_{2.85-\delta}F_{0.15}$	60	380	This work
H-$Sr_2Co_2O_5$	71	434	This work
IrO_2	62	348	This work
$LaCoO_3$	180	470	***Chem*** *3,**2017**, 812–821,*
$Sr_3FeCoO_{7-\delta}$	77	426	***J. Mater. Chem. A**, **2018**, 6, 14240–14245*
$NbBaMn_2O_{5.5}$	75	395	***ACS Catal**. **2018**, 8, 364–371*
$LaNi_{0.6}Fe_{0.4}O_3$	98	440	***Journal of The Electrochemical Society**, 165 (10) F827-F835 (**2018**)*
$Ba_{0.5}Sr_{0.5}Co_{0.8}Fe_{0.2}O_{3-\delta}$	80	464	***Electrochimica Acta** 246 (**2017**) 997–1003*
$La_{0.6}Sr_{0.4}Fe_{0.8}Co_{0.2}O_3$	-	420	***Journal of Electroanalytical Chemistry** 808 (**2018**) 412–419*
$Pr_{0.5}(Ba_{0.5}Sr_{0.5})_{0.5}Co_{0.8}Fe_{0.2}O_{3-\delta}$	91	387	***Adv. Energy Mater**. **2017**, 7, 1700666*

DFT Computational methods

We performed density functional theory (DFT) calculations using the Vienna *ab initio* simulation package (VASP)[1, 2]. The generalized gradient approximation (GGA) with the revised Perdew-Burke-Ernzelhoff (RPBE) functional was used to treat the exchanging correlation interaction[3], which is thought to give a better description of adsorption energies and was used in previous studies[4, 5]. To describe the well-known self-interaction of the 3d orbitals, like many previous DFT studies on $SrCoO_3$-based materials, GGA+U with U_{eff} = (U-J) = 3.3 eV was used to the Co 3d electrons[6-8]. The projector augmented wave (PAW) method with H ($1s^1$), O ($1s^2 2s^2 2p^4$), Co ([Ar]$3d^7 4s^2$), and Sr ([Kr]$5s^2$) was used to treat the ionic core electrons and valence electrons. The energy cutoff was set as 520 eV and the convergence criteria was 10^{-5} eV. Structure optimization was carried out till the force on each atom was less than 0.02 eV $Å^{-1}$. All the calculations were spin-polarized and ferromagnetic states were used.

The cubic $SrCoO_3$ material was based on a pseudocubic cell with 40 atoms ($Sr_8Co_8O_{24}$) that corresponds to a 2×2×2 supercell of the ideal cubic simple ABO_3 perovskite (Pm-3m) and the Brillouin zone integration was sampled with a 6×6×6 *Γ*-centered k-point grid. For the hexagonal bulk phase $Sr_2Co_2O_5$ ($Sr_{18}Co_{15}O_{45}$), a 6×6×4 *Γ*-centered k-point grid was used. The (001) surface of cubic $SrCoO_3$ and (0001) surface of hexagonal $Sr_2Co_2O_5$ are chosen to investigate the OER properties for those two materials. Adsorbed species were modeled using an eight-layer 2×2 slab with a vacuum separation of about 15 Å. For the corresponding 2×2 surface slab calculations, we used 4×4×1 *Γ*-centered k-point meshes. Experimental results have demonstrated that the oxygen non-stoichiometric value range of cubic SCO is 2.3~2.8 under room temperature. Based on this, we built a (001) surface of cubic SCO with 4 oxygen vacancies, corresponding to $Sr_{16}Co_{16}O_{44}$ ($SrCoO_{2.75}$) in addition to perfect cubic SCO surface. The (0001) surface of hexagonal SCO is consist of 18 Sr, 15 Co, and 45 O atoms, the same with the bulk SCO composition.

Here we consider the four electron reaction pathway:

H_2O (l) + * $\rightleftharpoons$ HO* + H^+ + e^- (1)

$\Delta G_1 = \Delta G_{HO*} - \Delta G_{H_2O(l)} - eU + k_b T \ln a_{H^+}$

HO* $\rightleftharpoons$ O* + H^+ + e^- (2)

$\Delta G_2 = \Delta G_{O*} - \Delta G_{HO*} - eU + k_b T \ln a_{H^+}$

O* + H_2O (l) $\rightleftharpoons$ HOO* + H^+ + e^- (3)

$\Delta G_3 = \Delta G_{HOO*} - \Delta G_{O*} - eU + k_b T \ln a_{H^+}$

HOO* $\rightleftharpoons$ O_2 (g) + H^+ + e^- + * (4)

$\Delta G_4 = \Delta G_{O_2} - \Delta G_{HOO*} - eU + k_b T \ln a_{H^+}$

From the above, the rate-determining step is the OER with the maximum free energy:

$G^{OER} = \max [\Delta G_1^0, \Delta G_2^0, \Delta G_3^0, \Delta G_4^0]$

For which $\Delta G_{1\text{-}4}^0$ is $\Delta G_{1\text{-}4}$ at U=0 (pH=14 and T=298.15 K).

Finally the theoretical overpotential can be obtained as:

$\eta^{OER} = G^{OER}/e - 1.23$ V

Notes and references

S1. P. E. Blöchl, *Physical review B*, 1994, **50**, 17953-17979.
S2. G. Kresse and J. Furthmüller, *Computational materials science*, 1996, **6**, 15-50.
S3. J. P. Perdew, K. Burke and M. Ernzerhof, *Physical review letters*, 1996, **77**, 3865-3868.
S4. I. C. Man, H. Y. Su, F. Calle-Vallejo, H. A. Hansen, J. I. Martínez, N. G. Inoglu, J. Kitchin, T. F. Jaramillo, J. K. Nørskov and J. Rossmeisl, *ChemCatChem*, 2011, **3**, 1159-1165.
S5. H. A. Tahini, X. Tan, U. Schwingenschlögl and S. C. Smith, *ACS Catalysis*, 2016, **6**, 5565-5570.
S6. H. A. Tahini, X. Tan, W. Zhou, Z. Zhu, U. Schwingenschlögl and S. C. Smith, *Energy Storage Materials*, 2017, **9**, 229-234.
S7. S. Zhang, N. Han and X. Tan, *RSC Advances*, 2015, **5**, 760-769.
S8. X. Lei, B. Xu, C. Ouyang and K. Huang, *The Journal of Physical Chemistry C*, 2017, **121**, 24987-24993.